High Resolution pH_e Imaging of Rat Glioma Using pH-Dependent Relaxivity

Maria L. Garcia-Martin,[1] Gary V. Martinez,[1] Natarajan Raghunand,[1] A. Dean Sherry,[3] Shanrong Zhang,[3] and Robert J. Gillies[1]*

Previous studies using MR spectroscopy have shown that the extracellular pH (pH_e) of tumors is acidic compared to normal tissues. This has a number of important sequelae that favor the emergence of more aggressive and therapy-resistant tumors. New MRI methods based on pH-sensitive T_1 relaxivity are an attractive alternative to previous spectroscopic methods, as they allow improvements in spatial and temporal resolution. Recently, pH-dependent GdDOTA-4AmP^{5-} and a pH-independent analog, GdDOTP^{5-}, were used to image renal pH in mice. The current study has used a similar approach to image pH_e in rat gliomas. Significant differences were observed compared to the renal study. First, the relaxivity of GdDOTP^{5-} was found to be affected by the higher extracellular protein content of tumors. Second, the pixel-by-pixel analysis of the GdDOTP^{5-} and GdDOTA-4AmP^{5-} pharmacokinetics showed significant dispersion, likely due to the temporal fluctuations in tumor perfusion. However, there was a robust correlation between the maximal enhancements produced by the two boluses. Therefore, to account for the local time-courses differences, pH_e maps were calculated at the time of maximal enhancement in each pixel. Finally, the comparison of the pH_e and the time to maximal intensity maps revealed an inverse relationship between pH_e and tumor perfusion. Magn Reson Med 55:309–315, 2006.

Key words: acid-base; MRI; relaxivity; gadolinium; tumor, pH

Over the past decades, non-invasive imaging techniques have been developed to characterize the metabolic and physiologic environments of living tissues. An important application to emerge in this area has been the measurement of tumor pH using magnetic resonance. This application began early on with the acquisition of ^{31}P MR spectra, which provided information not only on the in vivo nucleoside triphosphate (NTP) levels, but also inorganic phosphate, P_i, whose chemical shift is pH dependent (1,2). A neutral-to-alkaline tumor pH calculated from the chemical shift of P_i has been reported in numerous ^{31}P MRS studies of human and animal tumors (i.e., 7.0–7.4). This was discrepant with previous microelectrode reports of an acid pH in tumors, and was not resolved until it was shown that P_i reported primarily the *intracellular* pH (3). The *extracellular* pH (pH_e) can be interrogated using an exogenous ^{31}P NMR reporter, 3-amino propylphosphonate, 3-APP (4). Studies with 3-APP have confirmed that the average pH_e of tumors is acidic, with values reaching as low as 6.0 (5).

However, ^{31}P investigations are limited in both spatial and temporal resolution. Even at high field, voxel size is limited to *ca.* $4 \times 4 \times 4$ mm^3, with a temporal resolution on the order of 5 min. An improvement in spatial resolution has been achieved using ^{1}H NMR and 2-imidazol-1-yl-3-ethoxycarbonyl-propionate, IEPA, which has a hydrogen attached to C-2 of the imidazole ring whose chemical shift is pH-sensitive (6). This compound is non-toxic and is membrane impermeant, and thus restricted to the extracellular compartment. Using magnetic resonance spectroscopic imaging (MRSI), IEPA has been used to measure pH_e in breast cancer tumors (7,8) and gliomas (9) with spatial resolution up to $1 \times 1 \times 1$ mm^3. These studies showed, for the first time, that the pH_e in tumors was heterogeneous, with differences in pH_e of as much as 0.5 pH unit across 8 mm in distance. The relationship between the low pH_e and perfusion has been inferred (see refs. (5,8), yet cannot be directly tested by this method due to differences in the spatial resolution between dynamic contrast MR images and MRSI. Although the use of IEPA has led to an increase in the understanding of tumor pH_e regulation, it still suffers from relatively poor spatial and temporal resolution.

In recent years, methods have been developed that allow pH to be rapidly determined at spatial resolutions comparable to standard MRI. These methods fall into two broad categories: magnetization transfer and relaxation enhanced contrast (10). Magnetization transfer can be achieved with either endogenous (11) or exogenous (12–14) hydrogen donors, and has great potential, as the contrast can be turned on or off through on- and off-resonance irradiation. Relaxation enhanced pH measurements involve the use of gadolinium-based contrast reagents (Gd-CR) whose relaxivity is pH dependent. A number of such compounds have been developed (15,16) where the relaxation enhancement is primarily achieved through increased hydrogen exchange rates at the lanthanide center. This approach was first used by Brindle's group (17), who realized that the ability to quantitatively determine pH_e with relaxivity required accurate knowledge of the Gd-CR concentration in each voxel. More recently, this approach has been used to measure the pH_e in kidneys using Gd-DOTA-4AmP^{5-} (18,19). In that study, the concentration of GdDOTA-4AmP^{5-} at a given time post-injection was as-

[1]Department of Biochemistry and Molecular Biophysics, Arizona Cancer Center, The University of Arizona, Tucson, AZ, USA.

[2]Department of Chemistry, The University of Texas at Dallas, Richardson, TX, USA.

[3]The Rogers Magnetic Resonance Center, Department of Radiology, University of Texas Southwestern Medical Center, Dallas, TX, USA.

Grant Sponsor: NCI; Grant Numbers: R01 Ca 077575 and R24 088578 to RJG. Grant Sponsor: Robert A. Welch Foundation; Grant Number: AT-584. Grant Sponsor: National Institutes of Health; Grant Number: CA-84697. Grant Sponsor: Division of Research Resources and the National Institutes of Health; Grant Number: RR-02584 to ADS.

*Correspondence to: Robert J. Gillies, Department of Biochemistry and Molecular Biophysics, Arizona Cancer Center; 1515 N. Campbell Ave., Tucson, AZ, USA 85724-5024. E-mail: rgillies@email.arizona.edu

Received 11 July 2005; revised 3 October 2005; accepted 14 October 2005.
DOI 10.1002/mrm.20773
Published online 9 January 2006 in Wiley InterScience (www.interscience.wiley.com).

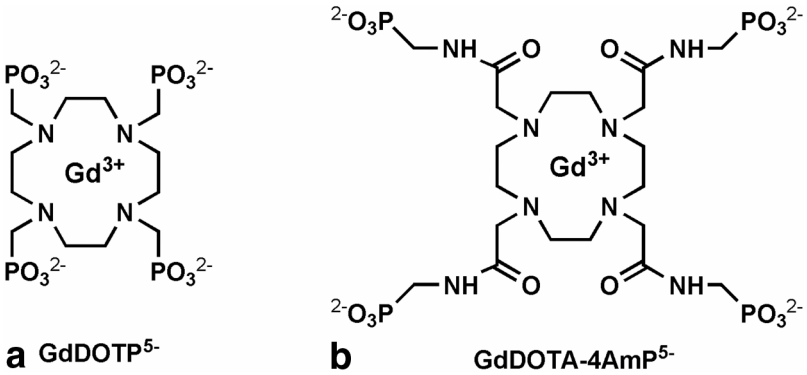

FIG. 1. Gadolinium chelates used for pH_e imaging: (**a**) pH-insensitive $GdDOTP^{5-}$, (**b**) pH-sensitive Gd-DOTA-$4AmP^{5-}$.

sumed equal to the concentration of pH-independent Gd-$DOTP^{5-}$ at the same time following a prior injection in the same animal. The renal pharmacokinetics of $GdDOTP^{5-}$ and the structurally dissimilar Gd-$DTPA^{2-}$ were shown to be identical in mice. Since $GdDOTP^{5-}$ and GdDOTA4AmP^{5-} are more closely related in charge and structure, it was assumed that they would also display identical renal pharmacokinetics.

The current study describes the continued use of this approach, *mutatis mutandis*, to measure pH_e in tumors. Using this strategy in tumors is significantly more difficult than in kidneys, owing to the notoriously heterogeneous distribution of patent blood vessels, slower wash-in and wash-out of i.v. delivered agents, and higher protein content of extracellular fluid. Despite these difficulties, accurate pH_e maps were generated and validated by comparison to IEPA results from the same model, as well as a rigorous analysis of the times to maximal intensity (TMI) of the two paramagnetic contrast reagents. This analysis allowed local time-dependent alterations in tumor perfusion to be identified and corrected before calculating the pH_e maps. The comparison of pH_e and TMI, which is a measure of tumor perfusion, revealed an inverse relationship between these two parameters.

METHODS

Cell Lines and Tumors

Rat C6 glioma cells (ATCC, CCL-107) were grown in Dulbecco's modified Eagle's medium (DMEM, Sigma, St. Louis, MO, USA) supplemented with 10% fetal bovine serum (FBS, Omega Scientific Inc., Tarzana, CA, USA). Gliomas were produced in female Wistar rats (200–250 g in body weight) by stereotaxic injection of 10^5 C6 cells in the right caudate nucleus (20). The rats were anesthetized with ketamine/xylazine (80/10 mg kg^{-1}, respectively, I.P.) and placed in a stereotaxic apparatus. After exposing the skull by a midline scalp incision, a 1 mm hole was drilled at 3.5 mm right from bregma and the cells were injected at a depth of 5.5 mm. To finish, the craniotomy was sealed with dental cement and the scalp sutured. Tumors developed for 2 to 3 weeks, occupying then up to 50% of the right hemisphere. All animal protocols were approved by the University of Arizona Institutional Animal Care and Use Committee.

In Vitro MRI Experiments

Solutions of $GdDOTP^{5-}$ and GdDOTA-$4AmP^{5-}$ were prepared in both phosphate buffered saline (PBS) and fetal bovine serum (FBS) at concentrations ranging from 0 to 5 mM and pH from 5 to 8.5. All the NMR measurements were carried out at 37°C and 4.7 T using the same experimental setting as for the in vivo experiments. T_1 was determined using an inversion-recovery sequence, with recovery delays from 20 to 12,000 ms. The T_1 relaxivities were then determined by fitting the experimental data to the following equation:

$$\frac{1}{T_1} = \frac{1}{T_{10}} + r_1[Gd] \quad [1]$$

where T_1 and T_{10} are the longitudinal relaxation times of water in the presence and absence of CR, respectively; and [Gd] is the concentration of the CR.

In Vivo MRI Experiments

Experiments were performed on a Bruker Biospec Avance® 4.7 T instrument equipped with 200mT/m actively shielded gradients. An 18 mm diameter surface coil positioned above the head of the rat was used for signal reception, and a 73 mm inner diameter volume resonator was used for excitation.

Animals were anesthetized with 1.5% (v/v) isoflurane in O_2 at 1L/min and then placed in a homemade holder equipped with ear bars to immobilize the head. Both rectal temperature and respiration rate were monitored all through the experiment. Temperature was maintained at 37–37.5°C by recirculating warm water. Two CRs, the pH-insensitive $GdDOTP^{5-}$ (Macrocyclics, Dallas, TX, USA, Fig. 1a) and the pH-sensitive GdDOTA-$4AmP^{5-}$ (Macrocyclics, Fig. 1b), were injected through the tail vein at an infusion rate of 0.24 $mmol{\cdot}Kg^{-1}{\cdot}min^{-1}$ over a total injection time of 25 s. Prior to injection of any CR, proton density and T_1 weighted spin echo images were acquired using the following parameters: TR = 5 s (proton density) or 80 ms (T_1 weighted), TE = 6 ms, FOV = 4 mm, slice thickness = 1 mm, matrix size = 128 × 128. Following the injection of each CR, a dynamic series of 120 T_1 weighted images was acquired over 1 h.

pH_e was calculated for each pixel as previously described (19). Briefly, the concentration of $GdDOTP^{5-}$ was determined as follows:

$$[GdDOTP] = \frac{1}{T_R r_{1,GdDOTP}} \mathrm{Ln}\frac{1-(I_{B,GdDOTP}/I_0)}{1-(I_{A,GdDOTP}/I_0)}[5] \quad [2]$$

where *TR* is the repetition time for the T_1 weighted image, r_1 is T_1 relaxivity of $GdDOTP^{5-}$ determined in vitro, $I_{B,GdDOTP}$ and $I_{A,GdDOTP}$ are the signal intensities on the T_1 weighted images before and after the injection of $GdDOTP^{5-}$, and I_O is the signal intensity on the proton density image. I_A corresponds to the maximal intensity in each pixel. The r_1 for $GdDOTA\text{-}4AmP^{5-}$ was determined from an analogous equation assuming the same concentration as $GdDOTP^{5-}$. The pH_e was then calculated according to the in vitro titration curve of pH_e versus r_1.

Data Analysis

The image processing software was developed in-house using Iterative Data Language (IDL; Research Systems, Boulder, CO, USA).

Statistical analysis of the relationship between pH_e and TMI was done by segmentation, using the CHAID (Chi-squared Automatic Interaction Detection) algorithm developed by Kass (21) as implemented in the SPSS AnswerTree Program (SPSS Inc. Headquarters, Chicago, IL, USA). CHAID allows the identification of cut-points for the independent (predictor) variables that lead to a statistically significant discrimination in the dependent measurement. This way a classification tree is generated where the tree trunk is all of the initial data and the branches are the subgroups delimited by the cut-points. ANOVA and non parametric analysis were done to ensure that extreme values did not affect the results.

RESULTS

In Vitro Calibration

The T_1 relaxivities (r_1) of $GdDOTP^{5-}$ and $GdDOTA\text{-}4AmP^{5-}$ were determined in PBS at different pH values at 37°C and 4.7 T. The T_1 relaxivity value obtained for $GdDOTP^{5-}$ in PBS was $3.2 \pm 0.04\ mM^{-1}\ s^{-1}$, which is in good agreement with previously published values (22). The T_1 relaxivity of $GdDOTP^{5-}$ was pH-independent whereas the $GdDOTA\text{-}4AmP^{5-}$ relaxivity was, as expected, strongly dependent on pH (Fig. 2). The experimental data were fit to a Hill-modified Henderson Hasselbach equation:

$$pH = 6.87 + \frac{\left[\dfrac{6.91 - r_{1,GdDOTA-4AmP}}{r_{1,GdDOTA-4AmP} - 3.45}\right]}{1.28}\ [7] \qquad [3]$$

Although the relaxivities measured in buffered aqueous solutions like PBS are frequently assumed to be a good approximation to the in vivo situation, recent studies have shown that macromolecular content can have a significant effect on the relaxivities of Gd chelates commonly used in clinical MRI (23). Therefore, the effect of macromolecules binding on the relaxivities of both $GdDOTP^{5-}$ and $GdDOTA\text{-}4AmP^{5-}$ was investigated by using fetal bovine serum, FBS, instead of PBS as solution media. The T_1 relaxivity of $GdDOTP^{5-}$ in 100% FBS was $5.7 \pm 0.1\ mM^{-1}\ s^{-1}$, higher than in PBS ($3.2 \pm 0.04\ mM^{-1}\ s^{-1}$). However, the r_1 relaxivities of $GdDOTA\text{-}4AmP^{5-}$ were not statistically different in the two solutions. The r_1 of $GdDOTP^{5-}$ determined in FBS was used for the in vivo data analysis.

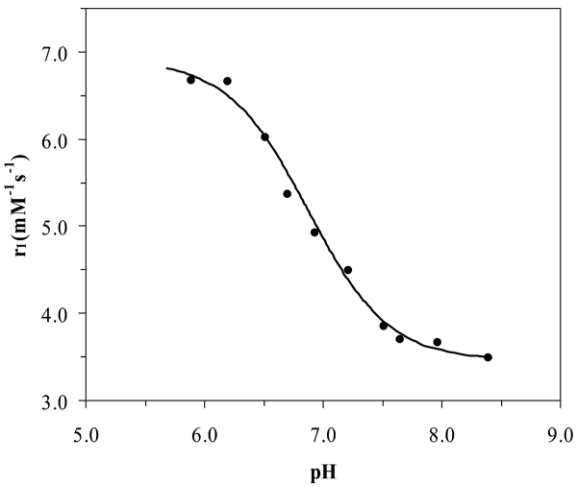

FIG. 2. Dependence of $GdDOTA\text{-}4AmP^{5-}$ T_1 relaxivity on pH (37°C, 4.7 T). The dots represent experimental data and the solid line the best fit to the Hill-modified Henderson Hasselbach equation: $pH = 6.87 + \log((6.91 - r_1)/(r_1 - 3.45))/1.28$.

Reproducibility of Pharmacokinetics

The R_1 relaxation enhancement produced by $GdDOTA\text{-}4AmP^{5-}$ in vivo depends on both contrast reagent concentration and extracellular pH. Therefore, in order to calculate the extracellular pH, an independent measurement of the CR concentration is needed. The current experimental protocol addressed this matter by using the pH-insensitive contrast reagent $GdDOTP^{5-}$, which was injected prior to the pH-sensitive $GdDOTA\text{-}4AmP^{5-}$, assuming that both CRs have identical pharmacokinetics. This approach has been successfully applied to mouse kidney studies (19). However, tumors are much more heterogeneously perfused as compared to kidneys, which may lead to spatially and temporally heterogeneous pharmacokinetics.

For this reason, special considerations have to be made in tumors as compared to other tissues. In particular, the influx and efflux in necrotic and/or poorly perfused areas can be slow and, consequently, some contrast reagent from the first bolus may still be present at the time of the second injection. To correct for residual $GdDOTP^{5-}$, a bi-exponential equation was fit on a pixel-by-pixel basis to the $GdDOTP^{5-}$ washout curve, and the extrapolated residue was subtracted from the $GdDOTA\text{-}4AmP^{5-}$ pharmacokinetics. To validate this approach, the same CR, GdDTPA, was injected sequentially, reasoning that the pharmacokinetics of both injections should be identical after correcting for residual enhancement. This is illustrated in Fig. 3, which shows average images corresponding to the first 10 min of acquisition following the first (Fig. 3a) and second (Fig. 3b) injections, as well as the difference between both of them before (Fig. 3c) and after (Fig. 3d) correcting for the residual enhancement. These experiments document the feasibility of performing two subsequent injections, 1 h apart, of a gadolinium-based contrast reagent, with reproducible pharmacokinetics. They also show that the residual enhancement from the first injection remaining in some parts of the tumor, like necrotic areas, can be predicted and corrected mathematically.

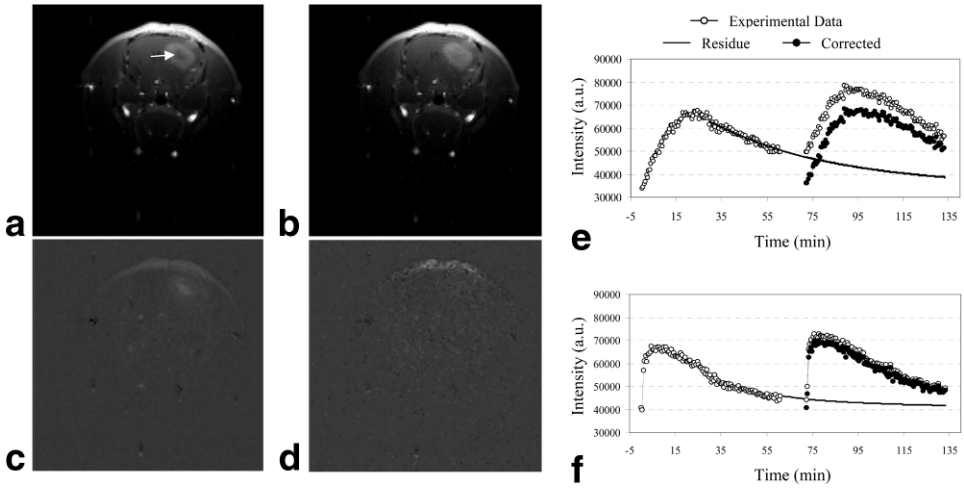

FIG. 3. Reproducibility of the pharmacokinetics of two successive bolus injections of GdDTPA. (**a**) and (**b**) average images corresponding to the first 10 min of the first and second pharmacokinetics, respectively; (**c**) difference image resulting from the subtraction of a from b; (**d**) difference image after correcting for the residual enhancement remaining from the first injection; (**e**) and (**f**) time courses of the two injections (empty circles), residue calculated by fitting a bi-exponential function to the decay of the first pharmacokinetics (solid line) and corrected pharmacokinetics after subtracting the residue (filled circles), in an ROI defined in the necrotic part of the tumor (pointed out by the arrow); (f) same as (e) but in the periphery of the tumor.

The pharmacokinetics of $GdDOTP^{5-}$ and GdDOTA-$4AmP^{5-}$ administered 1 h apart were compared by examining the time to maximal intensity (TMI) maps for both CRs. The TMI depends on the perfusion properties of the tumor, such as flow, vascular volume, volume of the extracellular/extravascular space, the extraction fraction, and the vascular permeability, as well as the CR pharmacokinetics and rate of renal clearance. Despite these complexities, TMI maps of CRs with similar pharmacokinetics were expected to be comparable for a given tumor.

To investigate this assumption, histograms of the time to maximal intensity of $GdDOTP^{5-}$ (TMI-1) and GdDOTA-$4AmP^{5-}$ (TMI-2) were generated and compared (Fig. 4). While not identical, these distributions in a single tumor were comparable. These data are shown in Table 1, where the mean TMI-1 and TMI-2 over the whole tumor are compared. The two-way ANOVA for repeated measures showed no significant difference ($P = 0.362$) between TMI-1 and TMI-2 when rats 1 and 8 were not included in the analysis. Therefore, only these two animals have significantly different TMI-1 and TMI-2, which may be due to differences in tumor perfusion during the second injection caused by depressed blood pressure during prolonged anesthesia (24). Changes in systemic blood pressure during the course of the experiment would not present a problem in studies of the kidneys, as in the previous study (19), due to powerful autoregulatory mechanisms designed to maintain stable renal blood flow over a wide range of perfusion pressures (25). However, tumor perfusion is directly dependent on systemic blood pressure.

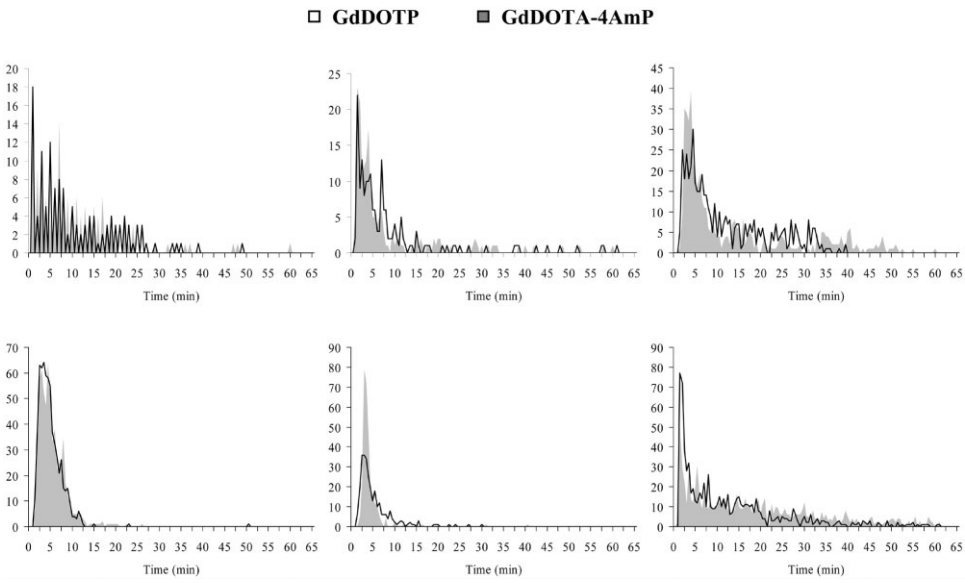

FIG. 4. Comparison of histograms from TMI-1 (black) and TMI-2 (gray) maps obtained after successive injections of Gd-$DOTP^{5-}$ and GdDOTA-$4AmP^{5-}$. Histograms were generated from a single ROI containing the tumor. The same ROI was used for both $GdDOTP^{5-}$ and GdDOTA-$4AmP^{5-}$ TMI maps in each animal. The 6 panels refer to 6 different animals.

The correlations between TMI-1 and TMI-2 were high for a 1 × 1 voxel ROI (Fig. 5), and were lower for a 128 × 128 data set. Hence, we reasoned that reduced resolution would yield improved correlations. Therefore, we subsequently investigated the effect of image resolution on the dispersion of the data by lowering the resolution of the raw images from 128 × 128 to 64 × 64 or 32 × 32 during post-processing, and recalculating both TMI and pH_e maps at each resolution. The correlations between TMI-1 and TMI-2 and between TMI-2 and pH_e were determined by calculating the Pearson product moment correlation coefficient (R) for each condition. These analyses revealed that the Pearson correlation coefficients between TMI of GdDOTP^{5-} and TMI of GdDOTA4AmP^{5-} increased from $R = 0.56$ to $R = 0.70$ as the image resolution decreased from 128 to 32. These correlation coefficients are low compared to $R = 0.96$ at an image resolution of 1 when the average TMI values over entire tumors were compared (Fig. 5). In-plane shifts due to motion were also investigated by generating one or two pixels shifted images in all directions and performing correlation analysis of the corresponding TMI maps. The results showed that no appreciable shifts occurred during the experimental time.

All together, these data indicate that even though the average pharmacokinetics of GdDOTP^{5-} and GdDOTA4AmP^{5-} averaged over the entire tumor are comparable, there are local differences within the tumor that give rise to higher dispersion on a pixel-by-pixel basis. In order to correct for these TMI differences, the pH maps were calculated at the maximal enhancement in each pixel, which shows a very good correlation between both contrast agents (Fig. 6).

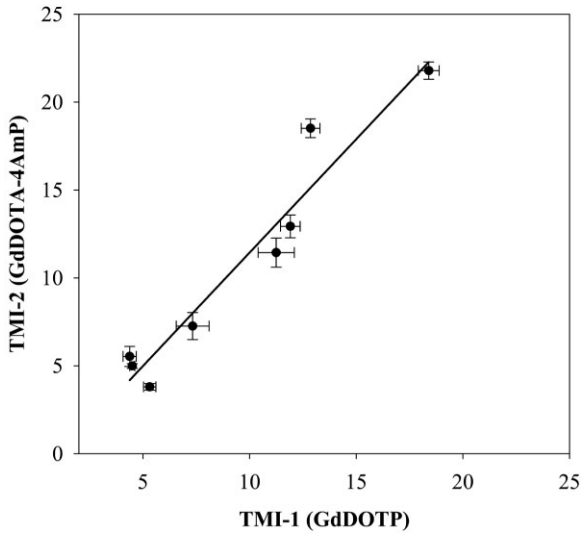

FIG. 5. Correlation between the average values of Time to Maximal Intensity after successive injections of GdDOTP^{5-} (TMI-1) and GdDOTA-4AmP^{5-} (TMI-2), over the entire tumor. Each point corresponds to the average value (± SEM) for one tumor, and the line shows the linear regression fit ($n = 8$, Pearson Correlation Coefficient = 0.966, $P < 0.0001$).

pH_e and TMI maps

Using the above calculations, high resolution pH_e and TMI maps were generated for C6 gliomas (Fig. 7). The pH_e was found to be heterogeneous throughout the tumor, with an overall mean of 6.87 ± 0.01 (± SE). This was more acidic than that observed for C6 gliomas in our previous studies (7.08 ± 0.017) using spectroscopic imaging methods (9). To examine the relationship between pH_e and perfusion, pH_e and TMI maps were compared on a pixel-by-pixel basis. First, linear correlation analyses were performed over the entire data set at different image resolutions showing low correlation coefficient, which did not improve significantly as the resolution decreased (data not shown). The mean pH and TMI over the entire tumor showed a higher correlation ($R = 0.7$), but was not statistically significant. Consequently, we applied segmentation analysis with Chi-squared Automatic Interaction Detection (CHAID), a non-parametric method that is useful to find non-linear relationships.

The segmentation analysis, illustrated in Fig. 8, revealed an inverse relationship between pH_e and TMI. Considering TMI as the independent variable, CHAID split the data into 3 subgroups of increasing TMI values (Fig. 8a): (i) TMI values lower or equal to 12.8 min, (ii) TMI values from 12.8 to 27.6 min, and (iii) TMI values higher than 27.6 min. Their corresponding mean pH_e values were 6.90, 6.84, and 6.73, respectively. Thus, pH_e decreased as the TMI increased. The differences among subgroups for both mean pH_e and mean TMI were confirmed to be statistically significant by performing ANOVA tests.

Table 1
Average Times to Maximal Intensity (min) Obtained After Successive Injections of GdDOTP^{5-} (TMI-1) and GdDOTA-4AmP^{5-} (TMI-2)

	GdDOTP^{5-}	GdDOTA-4AmP^{5-}
Rat 1	18.40 ± 16.02	21.79 ± 16.03
Rat 2	11.25 ± 9.81	11.44 ± 8.56
Rat 3	7.33 ± 10.88	7.26 ± 10.83
Rat 4	11.91 ± 9.05	12.93 ± 12.86
Rat 5	4.50 ± 3.10	4.99 ± 3.30
Rat 6	4.38 ± 4.07	5.53 ± 7.40
Rat 7	5.32 ± 5.07	3.80 ± 3.26
Rat 8	12.86 ± 12.76	18.51 ± 15.26

Values correspond to the mean (± standard deviation) calculated over the entire tumor. Data were compared by a two-way ANOVA test.

DISCUSSION

Previous work in our laboratory has established a dual injection technique for measuring pH_e in kidneys using pH-dependent relaxation of GdDOTA-4AmP^{5-} (19). The current study was designed to modify this approach for imaging pH_e in a well-perfused tumor model, C6 glioma. The assumption is made that the pH-sensitive GdDOTA-4AmP^{5-} and the pH-insensitive GdDOTP^{5-} have comparable pharmacokinetics and, hence, the concentration of the former can be inferred from the concentration of the latter. In good agreement with this assumption is the fact that the mean time to maximal intensity values over the whole tumor was statistically equal for both CRs in 75% of the tumors under study. In the remaining 25%, the overall tumor pharmacokinetics of GdDOTA-4AmP^{5-} was mea-

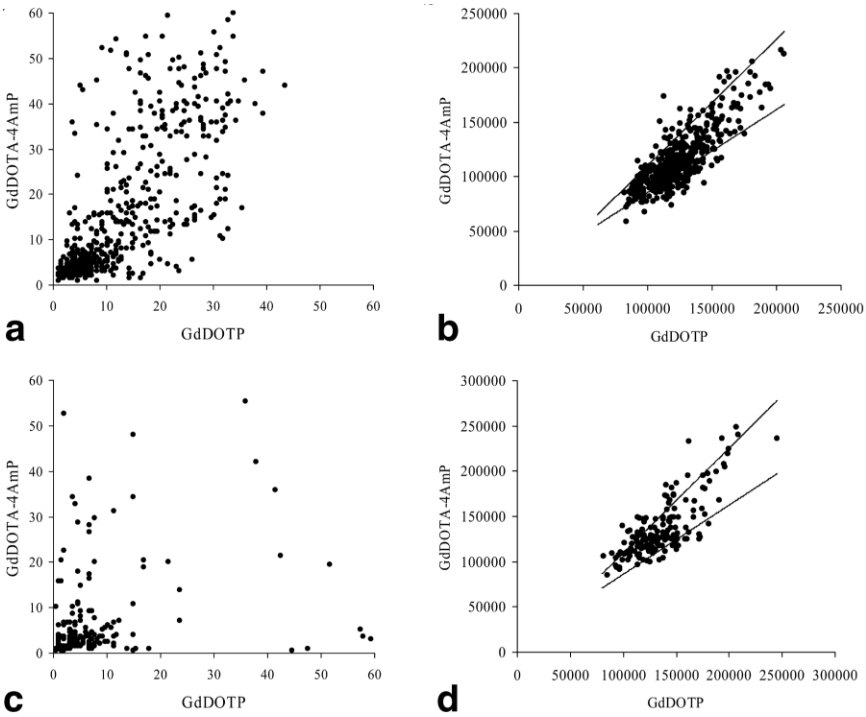

FIG. 6. Representative correlations between Time to Maximal Intensity (**a**,**c**) and Maximal Enhancement (**b**,**d**) after successive injections of GdDOTP^{5-} and GdDOTA-4AmP^{5-}. Upper and lower panels belong to 2 different animals. Dots represent experimental data, while lines show the theoretical relationship between the intensities of GdDOTP^{5-} and GdDOTA-4AmP^{5-} for pH = 5.8 (upper line) and pH = 7.3 (lower line).

sured to be slower than that of GdDOTP^{5-}, administered an hour earlier. A similar observation has recently been made with subsequent injections of Gd-DTPA (26). This is likely due to systemic reductions in blood pressure during prolonged anesthesia, as previously noted (24,27).

Although the pharmacokinetics of successive injections were highly correlated over the entire tumor, the correlations were substantially reduced when data were parsed on a pixel-by-pixel basis. This was not due to subject motion, as voxel shifting failed to increase correlations coefficients. Hence, we conclude that tumor perfusion is time-dependent on a microenvironmental scale. This is consistent with observations of Dewhirst and co-workers using window chamber models (28,29) and by Gallez using gradient echo imaging (30). In spite of the local temporal differences in tumor perfusion, accurate pH_e maps could be obtained by using the maximal enhancement in each pixel. The maximal enhancement is time independent and showed very good correlation for both CRs on a pixel-by-pixel-basis. When analyzed by automatic χ^2 routines, pH_e showed a statistically significant inverse relationship with TMI, indicating that more poorly perfused volumes (i.e., longer TMI) had lower pH_e.

In conclusion, a dual injection method was employed to obtain pH_e images in a well-perfused glioma model, and these showed an inverse relationship with perfusion. This approach allowed pH_e maps to be obtained with improved spatial resolution as compared to spectroscopic methods. However, the current protocol still suffers from poor temporal resolution, which needs to be improved with the aim of implementing this technique in a clinical setting. For

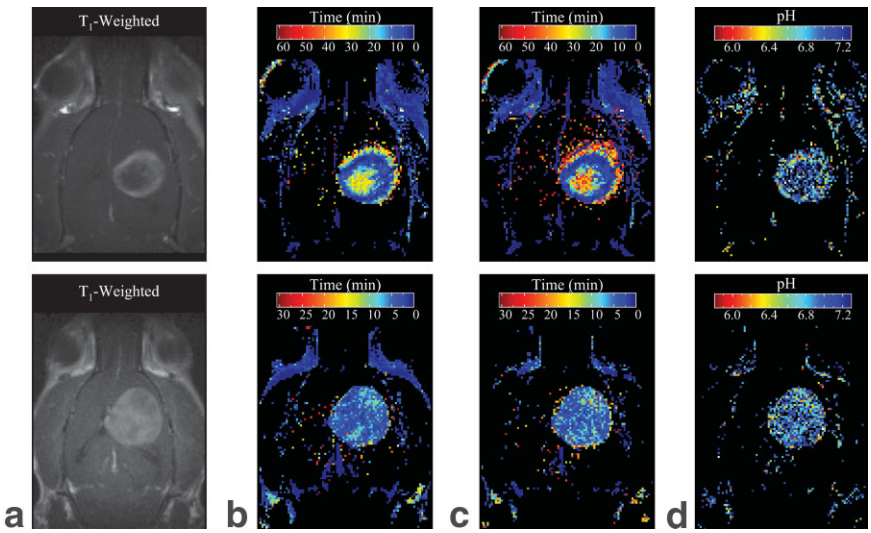

FIG. 7. Representative Time to Maximal Intensity (TMI) and pH_e maps in C6 gliomas in vivo. Upper and lower panels correspond to 2 different animals. (**a**) T_1-weighted images, (**b**) TMI maps of Gd DOTP^{5-}, (**c**) TMI maps of GdDOTA-4AmP^{5-}, (**d**) pH_e maps.

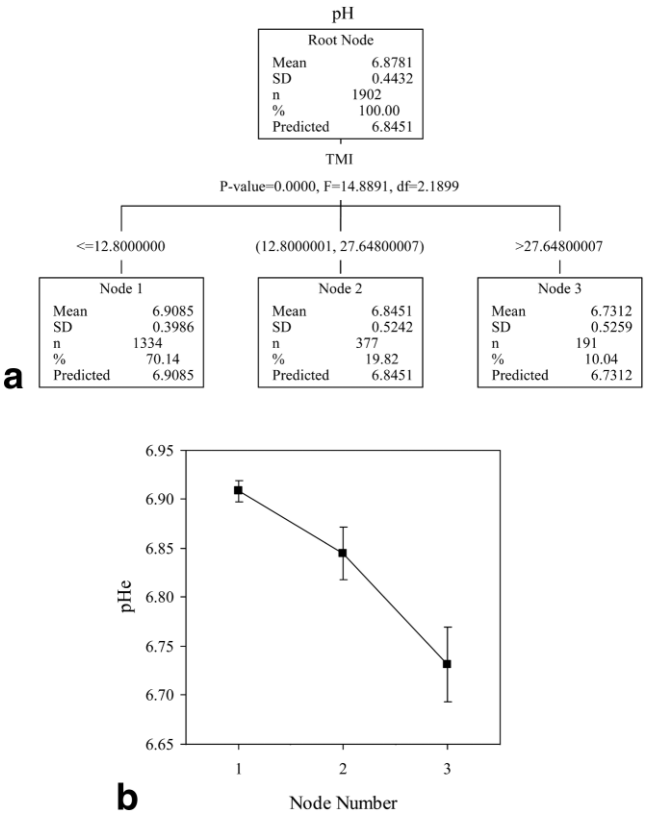

FIG. 8. CHAID-based segmentation analysis for the Time to Maximal Intensity obtained after the bolus injection of GdDOTA-4AmP^{5-} (TMI-2) and pH$_e$. (**a**) Classification tree for TMI-2 and pH$_e$, where TMI-2 and pH$_e$ correspond to the independent and dependent variables, respectively. (**b**) mean pH$_e$ (± SEM) for each TMI-2 subgroup number (nodes 1, 2, and 3).

this reason, continued research toward the development of single bolus pH imaging methods is warranted.

ACKNOWLEDGMENTS

The authors would like to acknowledge Brenda Baggett, Matt Runquist, Christine Howison, Fang Gao, and Josef Vagner for technical assistance.

REFERENCES

1. Griffiths JR, Stevens AN, Iles RA, Gordon RE, Shaw D. 31P-NMR investigation of solid tumours in the living rat. Biosci Rep 1981;1:319–325.
2. Evanochko WT, Ng TC, Lilly MB, Lawson AJ, Corbett TH, Durant JR, Glickson JD. In vivo 31P NMR study of the metabolism of murine mammary 16/C adenocarcinoma and its response to chemotherapy, x-radiation, and hyperthermia. Proc Natl Acad Sci U.S.A 1983;80:334–338.
3. Griffiths JR. Are cancer cells acidic? Br J Cancer 1991;64:425–427.
4. Gillies RJ, Liu Z, Bhujwalla Z. 31P-MRS measurements of extracellular pH of tumors using 3-aminopropylphosphonate. Am J Physiol 1994; 267:C195–203.
5. Gillies RJ, Raghunand N, Karczmar GS, Bhujwalla ZM. MRI of the tumor microenvironment. J Magn Reson Imaging 2002;16:430–450.
6. Gil S, Zaderenzo P, Cruz F, Cerdan S, Ballesteros P. Imidazol-1-ylalkanoic acids as extrinsic 1H NMR probes for the determination of intracellular pH, extracellular pH and cell volume. Bioorg Med Chem 1994;2:305–314.
7. van Sluis R, Bhujwalla ZM, Raghunand N, Ballesteros P, Alvarez J, Cerdan S, Galons JP, Gillies RJ. In vivo imaging of extracellular pH using 1H MRSI. Magn Reson Med 1999;41:743–750.
8. Bhujwalla ZM, Artemov D, Ballesteros P, Cerdan S, Gillies RJ, Solaiyappan M. Combined vascular and extracellular pH imaging of solid tumors. NMR Biomed 2002;15:114–119.
9. Garcia-Martin ML, Herigault G, Remy C, Farion R, Ballesteros P, Coles JA, Cerdan S, Ziegler A. Mapping extracellular pH in rat brain gliomas in vivo by 1H magnetic resonance spectroscopic imaging: comparison with maps of metabolites. Cancer Res 2001;61:6524–6531.
10. Gillies RJ, Raghunand N, Garcia-Martin ML, Gatenby RA. pH imaging. A review of pH measurement methods and applications in cancers. IEEE Eng Med Biol Mag 2004;23:57–64.
11. Zhou J, Payen JF, Wilson DA, Traystman RJ, van Zijl PC. Using the amide proton signals of intracellular proteins and peptides to detect pH effects in MRI. Nat Med 2003;9:1085–1090.
12. Ward KM, Balaban RS. Determination of pH using water protons and chemical exchange dependent saturation transfer (CEST). Magn Reson Med 2000;44:799–802.
13. Zhang S, Winter P, Wu K, Sherry AD. A novel europium(III)-based MRI contrast agent. J Am Chem Soc 2001;123:1517–1518.
14. Aime S, Barge A, Delli Castelli D, Fedeli F, Mortillaro A, Nielsen FU, Terreno E. Paramagnetic lanthanide(III) complexes as pH-sensitive chemical exchange saturation transfer (CEST) contrast agents for MRI applications. Magn Reson Med 2002;47:639–648.
15. Zhang S, Wu K, Sherry AD. A novel pH-sensitive MRI contrast agent. Angew Chem Int Ed Engl 1999;38:3192–3194.
16. Rowland IJ, Murphy PS, Schwarz A, Botta M, Aime S, Leach MO. In vivo extracellular pH mapping at 1.5T using proton CSI. In: Proceedings of the 6th Annual Meeting of the ISMRM, Sydney, Australia, 1998; p. 654.
17. Beauregard DA, Parker D, Brindle KM. Relaxation-based mapping of tumor pH. In: Proceedings of the 6thAnnual Meeting of the ISMRM, Sydney, Australia. 1998; p. 653.
18. Raghunand N, Zhang S, Sherry AD, Gillies RJ. In vivo magnetic resonance imaging of tissue pH using a novel pH-sensitive contrast agent, GdDOTA-4AmP. Acad Radiology 2002;9 Suppl 2:S481–483.
19. Raghunand N, Howison C, Sherry AD, Zhang S, Gillies RJ. Renal and systemic pH imaging by contrast-enhanced MRI. Magn Reson Med 2003;49:249–257.
20. Kobayashi N, Allen N, Clendenon NR, Ko LW. An improved rat brain-tumor model. J Neurosurg 1980;53:808–815.
21. Kass GV. An exploratory technique for investigating large quantities of categorical data. Applied Statistics 1980;29:119–127.
22. Aime S, Botta M, Terreno E, Anelli PL, Uggeri F. Gd(DOTP)5-outer-sphere relaxation enhancement promoted by nitrogen bases. Magn Reson Med 1993;30:583–591.
23. Stanisz GJ, Henkelman RM. Gd-DTPA relaxivity depends on macromolecular content. Magn Reson Med 2000;44:665–667.
24. Baudelet C, Gallez B. Effect of anesthesia on the signal intensity in tumors using BOLD-MRI: comparison with flow measurements by Laser Doppler flowmetry and oxygen measurements by luminescence-based probes. Magn Reson Imaging 2004;22:905–912.
25. Lessard MR, Trepanier CA. Renal function and hemodynamics during prolonged isoflurane-induced hypotension in humans. Anesthesiology 1991;74:860–865.
26. Yankeelov TE, DeBusk LM, Luci JJ, Lin PC, Price RR, Gore JC. Reproducibility of the reference region method for the analysis of DCE-MRI data. In: Proceedings of the 13th Annual Meeting of the ISMRM, Miami Beach, FL, USA, 2005. p. 2103.
27. Lukasik VM, Gillies RJ. Animal anaesthesia for in vivo magnetic resonance. NMR Biomed 2003;16:459–467.
28. Braun RD, Lanzen JL, Dewhirst MW. Fourier analysis of fluctuations of oxygen tension and blood flow in R3230Ac tumors and muscle in rats. Am J Physiol 1999;277:H551–568.
29. Kimura H, Braun RD, Ong ET, Hsu R, Secomb TW, Papahadjopoulos D, Hong K, Dewhirst MW. Fluctuations in red cell flux in tumor microvessels can lead to transient hypoxia and reoxygenation in tumor parenchyma. Cancer Res 1996;56:5522–5528.
30. Baudelet C, Ansiaux R, Jordan BF, Havaux X, Macq B, Gallez B. Physiological noise in murine solid tumours using T2*-weighted gradient-echo imaging: a marker of tumour acute hypoxia? Phys Med Biol 2004;49:3389–3411.